International Journal of Mechanical, Industrial and Aerospace Sciences
ISSN: 2517-9950
Vol:10, No:1, 2016

Free Convection in a Darcy Thermally Stratified Porous Medium That Embeds a Vertical Wall of Constant Heat Flux and Concentration

Maria Neagu

***Abstract*—**This paper presents the heat and mass driven natural convection succession in a Darcy thermally stratified porous medium that embeds a vertical semi-infinite impermeable wall of constant heat flux and concentration. The scale analysis of the system determines the two possible maps of the heat and mass driven natural convection sequence along the wall as a function of the process parameters. These results are verified using the finite differences method applied to the conservation equations.

***Keywords*—**Finite difference method, natural convection, porous medium, scale analysis, thermal stratification.

I. Introduction

THE natural convection triggered by a vertical semi-infinite impermeable wall embedded in a porous medium was intensively analyzed by scientific researchers in the last decades [1]-[22]. Due to the wide variety of its practical applications, different cases were considered, analyzed, and developed: the wall of constant [1]-[3] or variable [4], [5] temperature, constant [1] or variable [6] heat flux, constant [7]-[13] or variable concentration, constant concentration and variable heat flux [14], [15], variable heat and mass flux [16]; the non-Darcy porous medium [6], [17]; the dispersion effects analysis [7], [18]; the non-Newtonian fluid saturated porous medium [1], [16], [18]; the consideration of the Soret and the Dufour effects [15], [17]; the thermally [2]-[4], [8], [19]-[21] or the double stratified environment [22], etc. These analyses establish the heat and/or the mass transfer at the wall as well as the temperature, the concentration and the velocity fields in the boundary layer by using various methods: the scale analysis [1] ,[7], [10], [13], the similarity [3], [7], [10], [12]-[16], [18], [19] or the non-similarity [4], [5] techniques, the finite differences method [4], [8], [9], [11], [13], [15], the spline collocation method [2], [16], the fourth-order Runge-Kutta integration method [5], [10], [14], [17]-[19], etc. In this scientific environment, this paper establishes the succession of the heat and mass driven natural convection regimes that attain the equilibrium state along a vertical impermeable wall of constant heat flux and concentration, a wall that is embedded in a Darcy thermally stratified porous medium. While the scale analysis of the system reveals the order of magnitude of the boundary layers variables as well as the two possible natural convection regime sequences, the finite differences method is used to verify these results.

Maria Neagu is with the Department of Manufacturing Engineering, "Dunarea de Jos" University of Galati, 111 Domneasca Street, Galati 800201, Romania (phone: +(40) 336 130208, fax: +(40) 236 314463, e-mail: Maria.Neagu@ugal.ro).

II. Mathematical Formulation

A vertical semi-infinite impermeable wall embedded in a Darcy fluid- saturated porous medium is presented by Fig. 1 (a). The wall releases a uniform constant heat flux (q_w) and the concentration of a certain constituent is constant at the wall (C_w). The origin of the coordinate system is fixed at the leading edge of the wall, x and y being the vertical and horizontal coordinates, respectively. At a distance sufficiently far from the wall, y_∞, the environment temperature varies linearly with the vertical coordinate: $T_{\infty,x} = T_{\infty,0} + s_T x$, where s_T is the dimensional thermal stratification coefficient: $s_T = dT_{\infty,x}/dx$. The height of the computational domain is h. All the properties are constant except for the fluid density, ρ, that obeys the Boussinesq approximation: $\rho = \rho_0\left[1-\beta_T\left(T-T_{\infty,0}\right)-\beta_C\left(C-C_{\infty,0}\right)\right]$, where ρ_0 is the reference density, while β_T and β_C are the thermal and concentration expansion coefficient, respectively.

The governing equations of the system, after the elimination of the pressure terms, are:

$$\frac{\partial v}{\partial x}+\frac{\partial u}{\partial y}=0; \tag{1}$$

$$\frac{\partial v}{\partial y}-\frac{\partial u}{\partial x}=\frac{K}{\mu}\left(\rho g\beta_t\frac{\partial T}{\partial y}+\rho g\beta_c\frac{\partial C}{\partial y}\right); \tag{2}$$

$$\frac{\partial T}{\partial t}+v\frac{\partial T}{\partial x}+u\frac{\partial T}{\partial y}=\alpha\left(\frac{\partial^2 T}{\partial x^2}+\frac{\partial^2 T}{\partial y^2}\right); \tag{3}$$

$$\frac{\partial C}{\partial t}+v\frac{\partial C}{\partial x}+u\frac{\partial C}{\partial y}=D\left(\frac{\partial^2 C}{\partial x^2}+\frac{\partial^2 C}{\partial y^2}\right). \tag{4}$$

In (3) and (4), the following notations were used: u and v are the dimensional velocity components on the x and y directions, T–the dimensional temperature, C–the dimensional concentration, t–the dimensional time, g–the gravitational acceleration, K–the porous medium permeability, μ–the dynamic viscosity, α–the thermal diffusivity, D–the diffusion coefficient of the species.

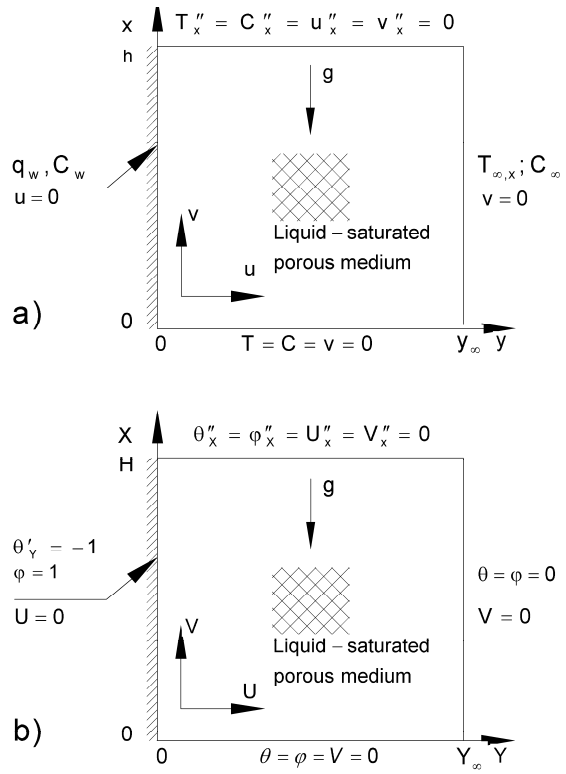

Fig. 1 (a) The vertical impermeable wall and the associated coordinate system; (b) the dimensionless domain of the problem

The following boundary conditions apply to (1)-(4):

$$u=0,\ \frac{\partial T}{\partial y}=-\frac{q_w}{k}=T_{x0},\ C=C_w \text{ at } y=0; \tag{5a}$$

$$v=0,\ T=T_{\infty,x},\ C=C_\infty \text{ as } y\to\infty; \tag{5b}$$

$$v=0,\ T=T_{\infty,x},\ C=C_\infty \text{ at } x=0; \tag{5c}$$

$$\frac{\partial^2 u}{\partial x^2}=\frac{\partial^2 v}{\partial x^2}=\frac{\partial^2 T}{\partial x^2}=\frac{\partial^2 C}{\partial x^2}=0 \text{ at } x=h \text{ [23]}, \tag{5d}$$

where k is the thermal conductivity of the porous medium.

The following non-dimensional variables of the Cartesian coordinates, temperature, and concentration, time, and velocity components are defined:

$$X=\frac{x}{L},\ Y=\frac{y}{L},\ \theta=\frac{T-T_{\infty,x}}{q_w L/k},\ \varphi=\frac{C-C_\infty}{C_w-C_\infty},$$

$$\tau=\frac{t\alpha}{L^2},\ U=\frac{u}{\alpha}L,\ V=\frac{v}{\alpha}L, \tag{6}$$

where L is an arbitrary characteristic length [23]. Fig. 1 (b) presents the dimensionless domain: $Y_\infty \times H$.

The governing equations in non-dimensional form:

$$\frac{\partial V}{\partial X}+\frac{\partial U}{\partial Y}=0; \tag{7}$$

$$\frac{\partial V}{\partial Y}-\frac{\partial U}{\partial X}=Ra\left(\frac{\partial \theta}{\partial Y}+N\frac{\partial \varphi}{\partial Y}\right); \tag{8}$$

$$\frac{\partial \theta}{\partial \tau}+V\frac{\partial \theta}{\partial X}+VS_T+U\frac{\partial \theta}{\partial Y}=\frac{\partial^2 \theta}{\partial X^2}+\frac{\partial^2 \theta}{\partial Y^2}; \tag{9}$$

$$\frac{\partial \varphi}{\partial \tau}+V\frac{\partial \varphi}{\partial X}+U\frac{\partial \varphi}{\partial Y}=\frac{1}{Le}\left(\frac{\partial^2 \varphi}{\partial X^2}+\frac{\partial^2 \varphi}{\partial Y^2}\right), \tag{10}$$

and the dimensionless boundary conditions:

$$U=0,\ \frac{\partial \theta}{\partial Y}=-1,\ \varphi=1 \text{ at } Y=0; \tag{11a}$$

$$V=0,\ \theta=\varphi=0 \text{ as } Y\to\infty; \tag{11b}$$

$$V=0,\ \theta=\varphi=0 \text{ at } X=0; \tag{11c}$$

$$\frac{\partial^2 U}{\partial X^2}=\frac{\partial^2 V}{\partial X^2}=\frac{\partial^2 \theta}{\partial X^2}=\frac{\partial^2 \varphi}{\partial X^2}=0 \text{ at } X=H, \tag{11d}$$

are determined by replacing (6) in (1)–(5). The following parameters occur in (7)–(11): $Ra=\left[Kg\beta_t(q_w/k)L^2/\alpha\nu\right]$, the Darcy–modified Rayleigh number based on heat flux, $N=\left[\beta_c(C_w-C_{\infty,0})/\beta_t(q_wL/k)\right]$, the buoyancy ratio, $S_T=\left[s_T/(q_wL/k)\right]$, the dimensionless thermal stratification parameter, and $Le=(\alpha/D)$, the Lewis number.

The scale analysis [24] of the dimensionless governing equations, (7)-(10), is realized in the following section, Section III. Section IV presents the numerical model used to solve the dimensionless governing equations and to verify the results established in Section III of this paper.

III. Scale Analysis

The initial moments, when the equilibrium state is not reached, are analyzed by Subsection A, while Subsections B and C present the scale analysis of the equilibrium state: B–the mass driven convection regime (MDC), C–the heat driven convection regime (HDC).

A. Scale Analysis of the Transient Stage

In the first moments, before the system reaches the equilibrium state, in the energy conservation equation, (9), the equilibrium between the inertia and the diffusion of heat in the Y direction is attained:

$$\frac{\partial \theta}{\partial \tau}\sim\frac{\partial^2 \theta}{\partial Y^2}. \tag{12}$$

As the temperature difference across the thermal boundary layer is $\Delta\theta$ and $Y \sim \delta_T$, the temperature boundary layer thickness in the transient regime, δ_T, becomes:

$$\delta_T \sim \tau^{1/2}. \quad (13)$$

Similarly, in the species conservation equation, (10), the equilibrium between the inertia and the diffusion in the Y direction, $\partial\varphi/\partial\tau \sim 1/Le \cdot \partial^2\varphi/\partial Y^2$, reveals the thickness of the concentration boundary layer, δ_C:

$$\delta_C \sim \tau^{1/2}/Le^{1/2}. \quad (14)$$

Assuming that the temperature and the concentration boundary layers thickness scale $\delta_T << X$ and $\delta_C << X$, we neglect the $\partial U/\partial X$ term in (8):

$$\frac{\partial V}{\partial Y} \sim Ra \cdot \left(\frac{\partial\theta}{\partial Y}\right) + Ra \cdot N \cdot \left(\frac{\partial\varphi}{\partial Y}\right). \quad (15)$$

Integrating (15) from $Y = 0$ to infinity, we obtain:

$$V \sim Ra \cdot \Delta\theta + Ra \cdot N \cdot \Delta\varphi. \quad (16)$$

Taking into account that the temperature difference across the temperature boundary layer is $\Delta T \sim T_{x0}\delta_T \sim T_{x0}\alpha^{1/2}t^{1/2}$ or $\Delta\theta \sim \tau^{1/2}$, the first term on the right hand side of (16) (V_T– the vertical velocity due to the buoyancy force that is determined by the volumetric thermal expansion) can be written as:

$$V_T \sim Ra \cdot (\Delta\theta) \sim Ra \cdot \tau^{1/2}. \quad (17)$$

The concentration difference across the concentration boundary layer is $\Delta C \sim (C_w - C_0)$ or $\Delta\varphi \sim 1$ and, consequently, the second term on the right hand side of (16) (V_C–the vertical velocity due to the buoyancy force that is determined by the volumetric concentration expansion) becomes:

$$V_C \sim Ra \cdot N \cdot (\Delta\varphi) \sim Ra \cdot N. \quad (18)$$

Using (16)–(18), the order of magnitude of the vertical velocity field is given by:

$$V \sim Ra \cdot \tau^{1/2} + Ra \cdot N. \quad (19)$$

The analysis of (19) shows that the V_T increases in time, while V_C is constant. Consequently, a mass driven convection (MDC) regime dominates initially at each X=constant level, but, if the equilibrium time, τ_{ech}, is bigger than the transition time, τ_{trz}:

$$\tau_{ech} < \tau_{trz} = N^2, \quad (20)$$

A heat driven convection (HDC) regime will be installed and it will reach the equilibrium state at that abscissa. It is the aim of this paper to establish the maps of the equilibrium mass and heat driven natural convection regimes that appear in the boundary layer near the vertical wall. In order to draw these maps, the scale analysis of the mass and heat driven convection regimes will be analyzed in the next two subsections.

B. Scale Analysis of the Mass Driven Convection (MDC) Regime

In the mass driven convection regime, the equilibrium is reached when the mass flux diffused in the Y direction equals the mass flux convected in the X direction:

$$V \cdot \frac{\Delta\varphi}{X} \sim \frac{1}{Le}\frac{\Delta\varphi}{\delta_C^2}. \quad (21)$$

The order of magnitude of the time when the equilibrium is attained is established by replacing the vertical velocity with the component dominant in the MDC regime, (18), and δ_C from (14):

$$\tau_C \sim X/(Ra \cdot N). \quad (22)$$

At this moment, according to (14), the concentration boundary layer thickness is:

$$(\delta_{ech,C})_C \sim [X/(Le \cdot Ra \cdot N)]^{1/2}. \quad (23)$$

The equilibrium time, τ_C, is bigger than the transition time, τ_{trz}, only if

$$X_{trz,C} = Ra \cdot N^3 < X. \quad (24)$$

Further, this study is completed by analyzing the temperature field in the mass driven convection regime.

C. Scale Analysis of the Temperature Field in the Mass Driven Convection Regime

For a complete understanding of the temperature field in the mass driven convection regime, the relative magnitude of the two vertical convective terms, $V \cdot S_T$ and $V \cdot \partial\theta/\partial X$, in the energy conservation equation, (9), must be analyzed. The $V \cdot S_T$ term is dominant if $S_t > \tau^{1/2}/X$ or

$$\tau < \tau_s = S_t^2 X^2. \quad (25)$$

As (25) tells us, at the beginning, when $\tau < \tau_s$, the $V \cdot S_T$ term is dominant but, in time, this situation remains unchanged or not depending on the relative magnitude of τ_s,

τ_{trz}, τ_C and the time when the temperature field attains the equilibrium state.

Further, the equilibrium time will be established for the two situations that could be encountered:

a) If (9) is characterized by the dominance of the $V \cdot \partial\theta / \partial X$ term, then, its scale analysis reveals that:

$$V \frac{\partial \theta}{\partial X} \sim \frac{\partial^2 \theta}{\partial Y^2}. \quad (26)$$

The time when the temperature field reaches the equilibrium state is found by replacing (18) and (13) in (26):

$$\left(\tau_{ech,T}\right)_C \sim X / \left(Ra \cdot N\right). \quad (27)$$

As we can notice, for this situation, the temperature and the concentration fields attain the equilibrium state in the same moment as τ_C, (22), and $\left(\tau_{ech,T}\right)_C$, (27), have the same form.

Using (13), at the equilibrium state, the temperature boundary layer thickness is:

$$\left(\delta_{ech,T}\right)_C \sim [\, X / \left(Ra \cdot N\right)]^{1/2}. \quad (28)$$

b) If the $V \cdot S_T$ term is the dominant vertical convection term in (9), then the scale analysis reveals that:

$$V \cdot S_T \sim \frac{\partial^2 \theta}{\partial Y^2}. \quad (29)$$

Using (13) and (18), we conclude that the moment when the equilibrium is attained has the order of magnitude $\left(\tau_{ech,St}\right)_C \sim \left[1/\left(Ra \cdot N \cdot S_t\right)\right]^2$ and that the magnitude of the equilibrium temperature boundary layer thickness is:

$$\left(\delta_{ech,St}\right)_C \sim 1/\left(Ra \cdot N \cdot S_t\right). \quad (30)$$

Further, the equilibrium time $\left(\tau_{ech,,St}\right)_C$ will be compared to τ_{trz} and τ_s:

b1) The equilibrium time $\left(\tau_{ech,,St}\right)_C$ is smaller than the transition time, τ_{trz}, on the domain defined by (31):

$$Ra \cdot N^2 \cdot S_T > 1. \quad (31)$$

b2) The possibility to have $\left(\tau_{ech,St}\right)_C < \tau_s$ is restricted to the domain defined bellow:

$$X > \frac{1}{Ra \cdot N \cdot S_T^2}. \quad (32)$$

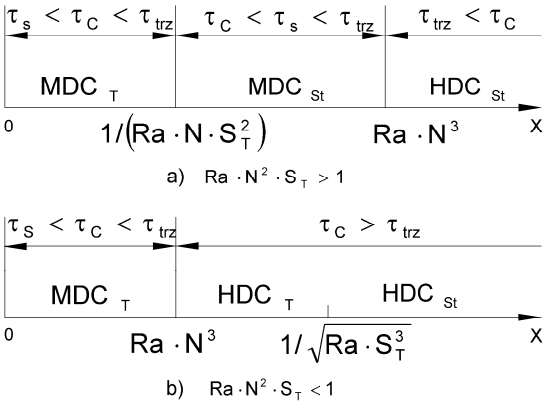

Fig. 2 The heat and mass driven natural convection regimes sequence a) $Ra \cdot N^2 \cdot S_T > 1$; b) $Ra \cdot N^2 \cdot S_T < 1$

Two distinct situations appear:

1. If (31) is valid, then the mass→heat driven convection transformation is taking place for abscissa greater than $X_{trz,C}$ ((24) and Fig. 2 (a)).

If (31) is valid, then the inequality $1/\left(Ra \cdot N \cdot S_T^2\right) < Ra \cdot N^3$ is also valid and, consequently, the $V \cdot S_T$ term remains the dominant vertical convection term in the heat transfer equation before the mass→heat driven convection transition is taking place in the $[1/\left(Ra \cdot N \cdot S_T^2\right), Ra \cdot N^3]$ domain (the MDC_{St} domain). The $V \cdot \partial\theta / \partial X$ term becomes the dominant vertical convection term in the $[0, 1/\left(Ra \cdot N \cdot S_T^2\right)]$ domain (the MDC_T domain). The regimes succession is presented by Fig. 2 (a): MDC_T — MDC_{St} — HDC_{St}.

2. If (31) is not valid, $1/\left(Ra \cdot N \cdot S_T^2\right) > Ra \cdot N^3$ and the mass→heat driven convection transition is taking place after the $V \cdot \partial\theta / \partial X$ term becomes dominant.

Fig. 2 (b) presents the regimes succession: MDC_T — HDC_T — HDC_{St}.

In order to establish the abscissa where the HDC_T — HDC_{St} transition is taking place, the scale analysis of the HDC regime is presented in the next section.

C. Scale Analysis of the Heat Driven Convection Regime

Two heat driven convection regime types : **HDC_{St}** regime (the $V \cdot S_T$ term is dominant and (25) is valid, Subsection *C* 1.) and **HDC** regime (the $V \cdot \partial\theta / \partial X$ term is dominant, Subsection *C* 2.) are encountered and they will be treated separately.

1. HDC_{St} Regime

The equilibrium state in the HDC_{St} regime is reached in the moment when the diffusion of heat away from the wall, in the *Y* direction, equals the convection of heat expressed by the $V \cdot S_T$ term:

$$V \cdot S_T \sim \frac{\partial^2 \theta}{\partial Y^2}. \quad (33)$$

Replacing (13) and (17) in (33), we obtain the equilibrium time:

$$\left(\tau_{ech,St}\right)_T \sim 1/\left(S_T \cdot Ra\right). \quad (34)$$

At this moment, the temperature boundary layer thickness is

$$\left(\delta_{ech,St}\right)_T \sim 1/\sqrt{S_T \cdot Ra}. \quad (35)$$

This state of equilibrium is attained before the transition $HDC_{St} \rightarrow HDC$ if $\left(\tau_{ech,St}\right)_T < \tau_s$ or

$$X > 1/\sqrt{Ra \cdot S_T^3}. \quad (36)$$

This is the condition that separates the HDC and HDC_{St} regimes in Fig. 2 (b).

For the $Ra \cdot N^2 \cdot S_T > 1$ case (Fig. 2 (a)), $1/\sqrt{Ra \cdot S_T^3} < Ra \cdot N^3$ and we can verify once again that a HDC_{St} regime is installed beyond $X_{trz,C}$ abscissa.

2. HDC Regime

In the region where the $V \cdot \partial\theta/\partial X$ term is dominant, the equilibrium state is characterized by: $V \cdot \Delta\theta / X \sim \Delta\theta / \delta_t^2$. The equilibrium time is:

$$\left(\tau_{ech,T}\right)_T \sim (X/Ra)^{2/3}. \quad (37)$$

and the thermal boundary layer thickness becomes:

$$\left(\delta_{ech,T}\right)_T \sim (X/Ra)^{1/3}. \quad (38)$$

D. Scale Analysis of the Concentration Field in the Heat Driven Convection Regime

The scale analysis of (10) reveals that $V \cdot \partial\varphi/\partial X \sim 1/Le \cdot \partial^2\varphi/\partial Y^2$. Using (14) and (17), the time when the concentration field attains the equilibrium state is: $\left(\tau_{ech,C}\right)_T \sim \left(X/Ra\right)^{2/3}$. The concentration boundary layer thickness is:

$$\left(\delta_{ech,C}\right)_T \sim 1/Le^{1/2}(X/Ra)^{1/3} \quad (39)$$

Imposing the condition for the thermal boundary layer approximation validity: $\left(\delta_{ech,St}\right)_C << 1/\left(RaNS_T^2\right)$ if $Ra \cdot N^2 \cdot S_T > 1$ or $\left(\delta_{ech,St}\right)_T << 1/\sqrt{RaS_T^3}$ if $Ra \cdot N^2 \cdot S_T < 1$, we obtain the same requirement: $S_T << 1.0$. As $\left(\delta_{ech,C}\right)_T < \left(\delta_{ech,C}\right)_C$ if $X > RaN^3$, the validity of the concentration boundary layer approximation, $\left(\delta_{ech,C}\right)_C << X$, imposes the condition: $X >> 1/\left(LeRaN\right)$ and it defines "a diffusive region" [23] that occurs for small values of X.

IV. Numerical Modeling

Using a stream function formulation for the velocity field: $U = -\partial\Psi/\partial X$, $V = \partial\Psi/\partial Y$, the new form of the dimensionless governing equations is given by (40)−(42):

$$\frac{\partial^2\Psi}{\partial Y^2} + \frac{\partial^2\Psi}{\partial X^2} = Ra \cdot \left(\frac{\partial\theta}{\partial Y} + N\frac{\partial\varphi}{\partial Y}\right); \quad (40)$$

$$\frac{\partial\theta}{\partial\tau} + \frac{\partial\Psi}{\partial Y}\frac{\partial\theta}{\partial X} + S_T\frac{\partial\Psi}{\partial Y} - \frac{\partial\Psi}{\partial X}\frac{\partial\theta}{\partial Y} = \frac{\partial^2\theta}{\partial X^2} + \frac{\partial^2\theta}{\partial Y^2}; \quad (41)$$

$$\frac{\partial\varphi}{\partial\tau} + \frac{\partial\Psi}{\partial Y}\frac{\partial\varphi}{\partial X} - \frac{\partial\Psi}{\partial X}\frac{\partial\varphi}{\partial Y} = \frac{1}{Le}\left(\frac{\partial^2\varphi}{\partial X^2} + \frac{\partial^2\varphi}{\partial Y^2}\right). \quad (42)$$

The following boundary conditions apply to (40)−(42):

$$\Psi = 0,\ \frac{\partial\theta}{\partial Y} = -1,\ \varphi = 1 \text{ at } Y = 0; \quad (43a)$$

$$\frac{\partial\Psi}{\partial Y} = 0,\ \theta = \varphi = 0 \text{ as } Y = L; \quad (43b)$$

$$\Psi = 0,\ \theta = \varphi = 0 \text{ at } X = 0; \quad (43c)$$

$$\frac{\partial^2\psi}{\partial X^2} = \frac{\partial^3\psi}{\partial X^3} = \frac{\partial^2\theta}{\partial X^2} = \frac{\partial^2\varphi}{\partial X^2} = 0 \text{ at } X = H. \quad (43d)$$

The governing equations, (40)-(42), subjected to the boundary conditions, (43), were solved numerically using the finite difference method, the higher order hybrid scheme – the "QUICK scheme" [25], [26]. Second-order finite-difference representation was used for all the terms of (40); third-order one-sided finite-difference representation was used for the convection terms at the boundary points in (41) and (42); the left boundary of (41) received a first-order finite-difference representation of (43a) using an external point. The influence of the number of the grid points, the upper limit of the computational domain, the time step and the variables relative error on the results (the Nusselt number, the Sherwood number, the values of the temperature and the concentration fields) was analyzed. The program was also tested with good results using the boundary conditions and the data already published in the literature [27]-[29].

V. Results and Discussions

The MDC_T—HDC_T—HDC_{St} regime sequence that is encountered for the $Ra \cdot N^2 \cdot S_T < 1$ case was verified using the $Ra = 300$, $N = 0.2$, $Le = 1$ and $S_T = 0.02$ case. A domain with $H = 25$ and $Y_\infty = 0.7$ was discretized using 1251×71 points uniformly distributed along the X and Y direction,

respectively, a situation that proved to assure a high accuracy of the results: the Nusselt and the Sherwood numbers have a precision higher than 2%, while the relative error for the temperature, concentration and stream function fields in each point is less than 10^{-6}. The results of Section III show that MDC_T—HDC_T transition takes place at the $Ra \cdot N^3 = 2.4$ abscissa and that the HDC_T—HDC_{St} transition occurs at $1/\sqrt{RaS_T^3} = 20.4$ abscissa. Fig. 3 presents the dimensionless temperature (Fig. 3 (a)), concentration (Fig. 3 (b)), and stream function (Fig. 3 (c) and $(\partial\theta/\partial X)/S_T$ (Fig. 3 (d)) fields for the considered case. Fig. 3 (a) shows values of the temperature field greater than 0.2 for $X \geq 1.84$ and, in this way, it reveals the MDC_T—HDC_T transition point. Fig. 3 (d) shows values of $(\partial\theta/\partial X)/S_T$ smaller than 1.0 for $X \geq 3.6$; it verifies the HDC_T—HDC_{St} transition. The difference between the analytical values (20.4) and the numerical value (3.6) of this transition abscissa is due to the approximations induced by the scale analysis method.

In the MDC_T region, Figs. 4 (a)-(c) present the temperature, concentration and vertical velocity fields for three abscissas: 0.67, 0.83; 1.0. Making use of (28), (23) and (18), Figs. 4 (d)-(f) present the scaled temperature, concentration and vertical velocity fields as a function of the scaled ordinate for the same abscissa. The collapse of these graphs on the same curve, proves the validity of the scaling dimensions determined previously.

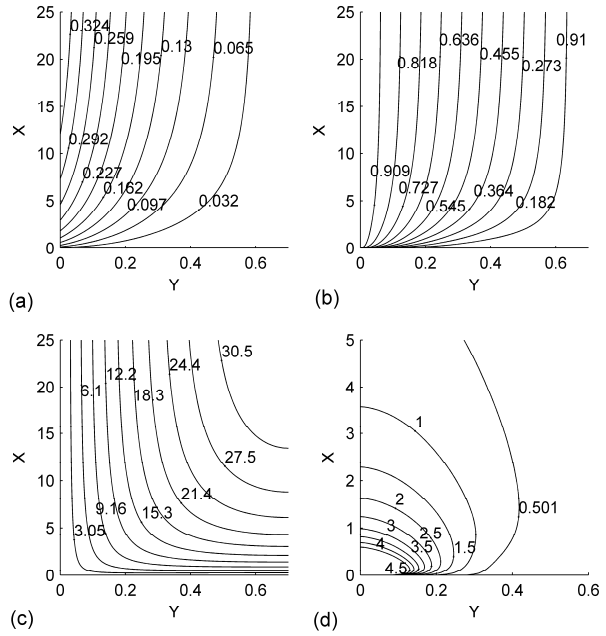

Fig. 3 (a) Dimensionless temperature (θ), (b) concentration (φ), (c) stream function (ψ) and (d) $(\partial\theta/\partial X)/S_T$ fields $Ra = 300$, $N = 0.2$, $Le = 1$ and $S_T = 0.02$

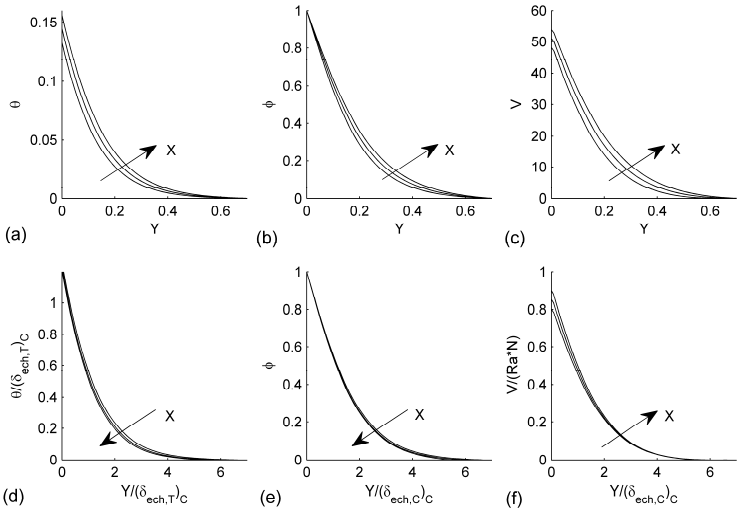

Fig. 4 (a) θ, (b) ϕ, and (c) V fields variations as a function of Y co-ordinate and the scaled (d) temperature, (e) concentration and (f) vertical velocity field variations as a function of scaled ordinate, for three abscissas: 0.63, 0.8 and 1.0, $Ra = 300$, $N = 0.2$, $Le = 1$ and $S_T = 0.02$

Figs. 5 (a)-(c) present the temperature, concentration and velocity fields for three abscissas: 2.67, 3.0 and 4.0 belonging to the HDC_T region. Figs. 5 (d)-(f) present the scaled temperature, concentration and vertical velocity fields as a function of the scaled ordinate for the same abscissas mentioned above and making use of the results given by (38), (39), (37) and (17).

Figs. 6 (a)-(c) present the temperature, concentration and velocity fields for the following abscissas: 21.0, 22.0 and 24.0 of the HDC_{St} region. For the same abscissas, using (35), (39), (34) and (17), Figs. 6 (d)-(f) present the scaled temperature, concentration and velocity fields as a function of the scaled ordinate giving a verification of the natural convection regime and the scaled defined for this region.

The $Ra \cdot N^2 \cdot S_T > 1$ case (Fig. 2 (a)), the MDC_T—MDC_{St}—HDC_{St} natural convection regimes sequence will be verified considering the $Ra = 600$, $N = 0.2$, $Le = 1$ and $S_T = 0.05$ system. A domain with $H = 6$ and $Y_\infty = 0.4$ was discretized using 606×46 points uniformly distributed, a situation that assures the same accuracy as for the previous case. The results of Section III indicate that the MDC_T—MDC_{St} transition takes place at the $1/\left(RaNS_T^2\right) = 3.34$ abscissa and that the MDC_{St}—HDC_{St} transition occurs at $Ra \cdot N^3 = 4.8$ abscissa. The numerical modeling results presented by Fig. 7 show that the $\left(\partial\theta / \partial X\right) / S_T$ values become smaller than 1.0 (i.e., the MDC_{St} regime occurs) for $X \geq 1.02$, while the temperature field has values greater than 0.2 (i.e., the MDC_{St}—HDC_{St} transition occurs) for $X \geq 4.4$.

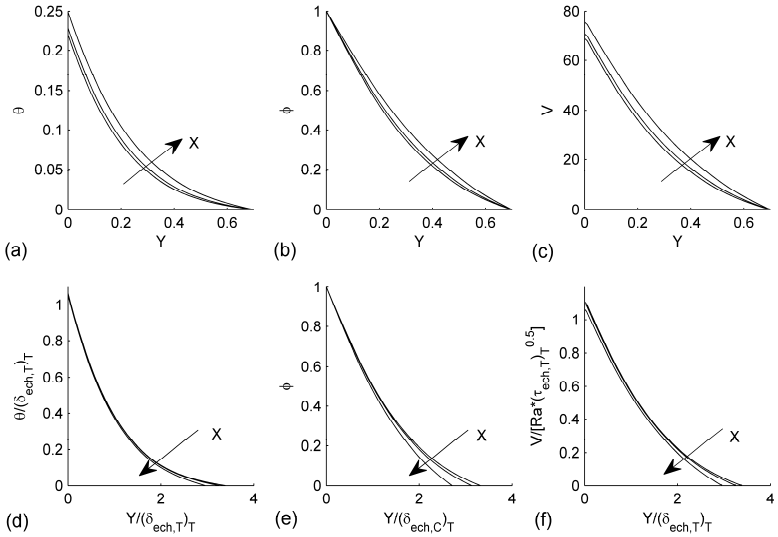

Fig. 5 (a) θ, (b) ϕ, and (c) V fields variations as a function of Y co-ordinate and the scaled (d) temperature, (e) concentration and (f) vertical velocity field variations as a function of scaled ordinate, for three abscissas: 2.67, 3.0 and 4.0, $Ra = 300$, $N = 0.2$, $Le = 1$ and $S_T = 0.02$

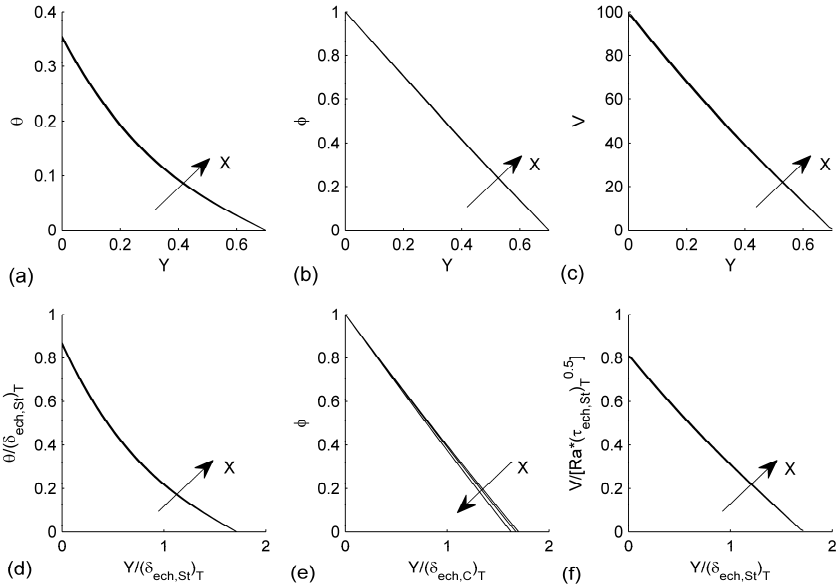

Fig. 6 (a) θ, (b) ϕ, and (c) V fields variations as a function of Y co-ordinate and the scaled (d) temperature, (e) concentration and (f) vertical velocity field variations as a function of scaled ordinate, for three abscissas: 21.0, 22.0 and 24.0, $Ra = 300$, $N = 0.2$, $Le = 1$ and $S_T = 0.02$

The MDC_T region and its scaling results were verified using the temperature, concentration and vertical velocity plots at the following abscissas: 0.5, 0.67 and 0.83 (Figs. 8 (a)-(c)), while Figs. 8 (d)-(f) present the scaled temperature,

concentration and velocity fields as a function of the scaled ordinate for the same abscissas. The collapse of these graphs on the same curve, prove the validity of the scaling dimensions determined previously.

Figs. 9 (a)-(c) present the temperature, concentration and vertical velocity fields for three abscissas: 3.5, 3.75 and 4.0 in the MDC_{St} section. Figs. 9 (d)-(f) present the scaled temperature, concentration and velocity fields as a function of the scaled ordinate making use of (30), (23) and (18).

The HDC_{St} region results were proved by plotting the temperature, concentration and velocity fields for the following abscissa: 5.0, 5.4 and 5.8 (Figs. 10 (a)-(c)). For the same abscissas, using the results given by (35), (39), (34) and (17), Figs. 10 (d)-(f) present the scaled temperature, concentration and vertical velocity fields as a function of the scaled ordinate giving a verification of the natural convection regime and the results obtained for this region.

The results presented by Figs. 3-10 prove the succession of the heat/mass transfer regimes for the two possible cases revealed by the scale analysis of the system.

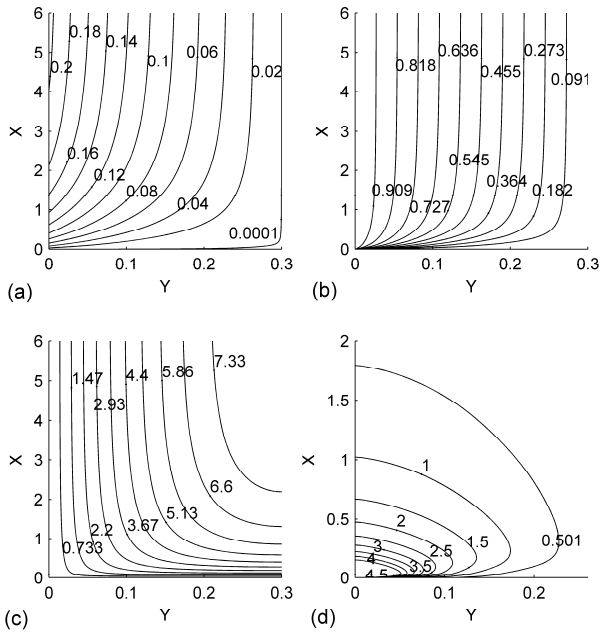

Fig. 7 (a) θ, (b) ϕ, (c) ψ, and (d) $(\partial\theta/\partial X)/S_T$ fields. $Ra = 600$, $N = 0.2$, $Le = 1$ and $S_T = 0.05$

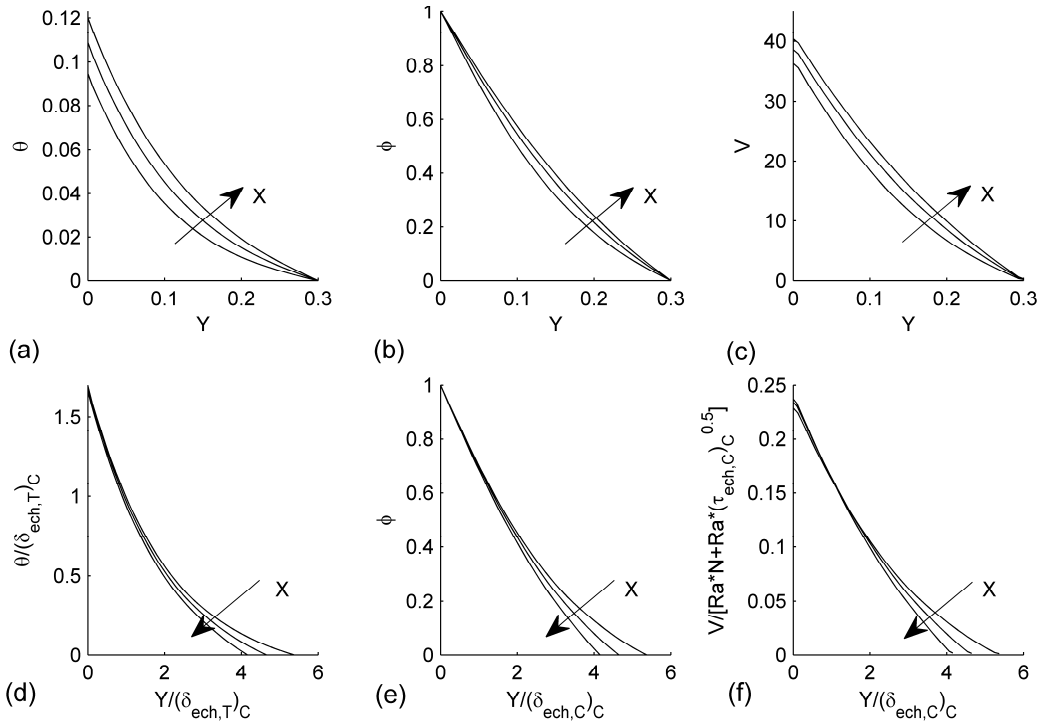

Fig. 8 (a) θ, (b) ϕ, and (c) V fields variations as a function of Y co-ordinate and the scaled (d) temperature, (e) concentration and (f) vertical velocity field variations as a function of scaled ordinate, for the abscissas: 0.50, 0.67 and 0.83, $Ra = 600$, $N = 0.2$, $Le = 1$ and $S_T = 0.05$

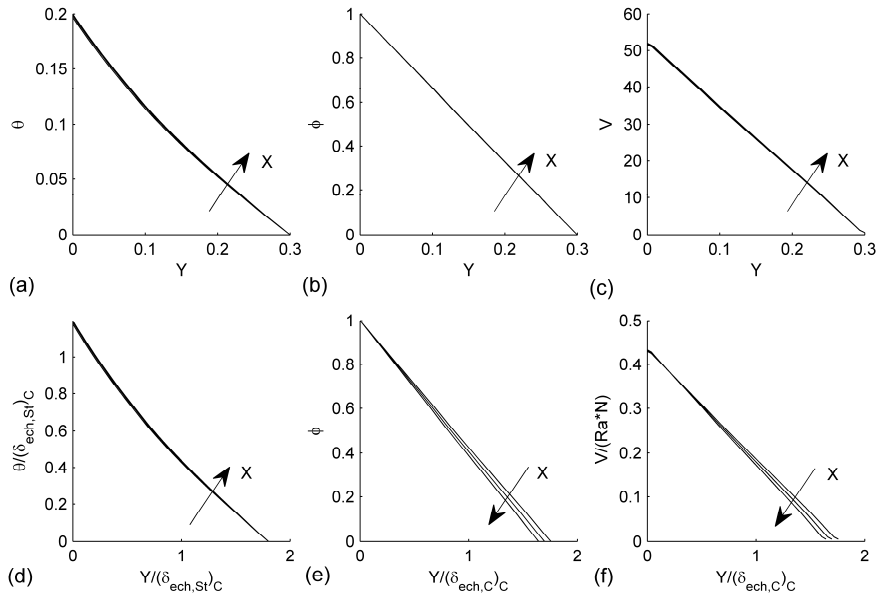

Fig. 9 (a) θ, (b) ϕ, and (c) V fields variations as a function of Y co-ordinate and the scaled (d) temperature, (e) concentration and (f) vertical velocity field variations as a function of scaled ordinate, for three abscissas: 3.5, 3.75 and 4.0, $Ra = 600$, $N = 0.2$, $Le = 1$ and $S_T = 0.05$

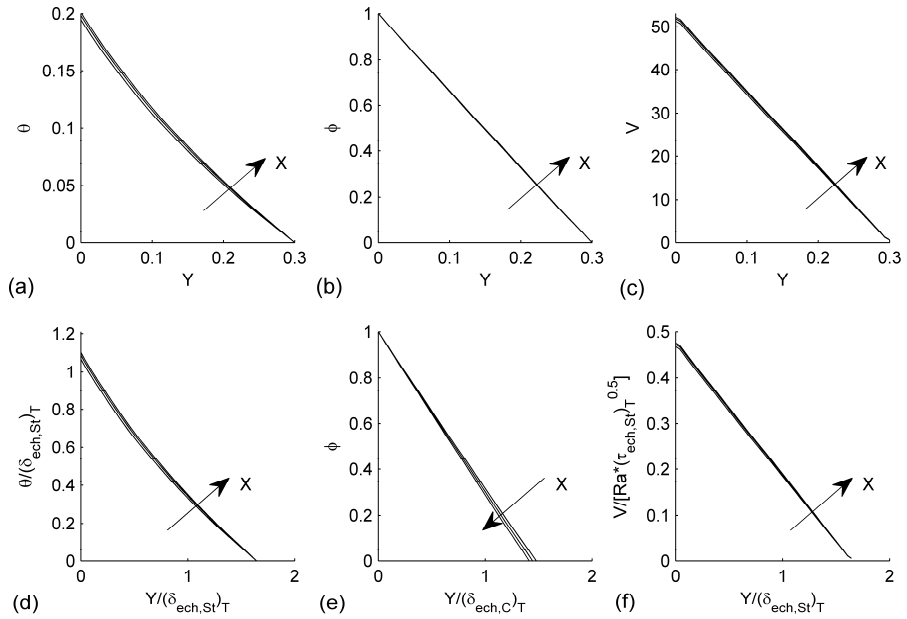

Fig. 10 (a) θ, (b) ϕ, and (c) V fields variations as a function of Y co-ordinate and the scaled (d) temperature, (e) concentration and (f) vertical velocity field variations as a function of scaled ordinate, for three abscissas: 5.0, 5.4 and 5.8, $Ra = 600$, $N = 0.2$, $Le = 1$ and $S_T = 0.05$

VI. Conclusion

The natural convection process that is taking place in a fluid-saturated Darcy thermally stratified porous medium that embeds a vertical impermeable wall of constant heat flux and concentration is an array of mass and heat driven convection regimes that attain the equilibrium state along the wall.

If $Ra \cdot N^2 \cdot S_T > 1$, after the first region, where a mass driven convection regime (MDC_T) is present, an intermediate MDC_{St} regime is followed by an HDC_{St} regime.

If $Ra \cdot N^2 \cdot S_T < 1$, then, at equilibrium, after the first MDC_T region, we encounter a HDC_T region followed by an HDC_{St} region.

This paper brings a new understanding of the important natural convection process triggered in a fluid-saturated

thermally stratified porous medium by a vertical impermeable wall of constant heat flux and concentration. This work triggers similar analysis regarding a doubly stratified Darcy porous medium, a vertical wall of constant temperature and mass flux, etc.

REFERENCES

[1] G. Degan, C. Akowanou, N. C. Awanou, "Transient natural convection of non-Newtonian fluids about a vertical surface embedded in an anisotropic porous medium," *International Journal of Heat and Mass Transfer*, vol. 50, no. 23−24, pp. 4629−4639, 2007.

[2] C. 'O.-K. Chen, C.-R. Lin, "Natural convection from an isothermal vertical surface embedded in a thermally stratified high-porosity medium," *International Journal of Engineering Science*, vol. 33, no. 1, pp. 131−138, 1995.

[3] K. Tewari. P. Singh, "Natural convection in a thermally stratified fluid saturated porous medium," *International Journal of Engineering Science*, vol. 30, no. 8, pp. 1003−1007, 1992.

[4] C.-I. Hung, C.-H. Chen, C.-B. Chen, "Non-Darcy free convection along a nonisothermal vertical surface in a thermally stratified porous medium," *International Journal of Engineering Science*, vol. 37, no. 4, pp. 477−495, 1999.

[5] F. C. Lai, "Non-Darcy natural convection from a line source of heat in saturated porous medium," *International Communications in Heat and Mass Transfer*, vol. 18, no. 4, pp. 445−457, 1991.

[6] Z. H. Kodah, A. M. Al-Gasem, "Non-Darcy mixed convection from a vertical plate in saturated porous media-variable surface heat flux," *Heat and Mass Transfer* , vol. 33, no. 5−6, pp. 377−382, 1998.

[7] R. S. Telles, O. V. Trevisan, "Dispersion in heat and mass transfer natural convection along vertical boundaries in porous media," *International Journal of Heat and Mass Transfer*, vol. 36, no. 5, pp. 1357−1365, 1993.

[8] D. Angirasa, G. P. Peterson, "Natural convection heat transfer from an isothermal vertical surface to a fluid saturated thermally stratified porous medium," *International Journal of Heat and Mass Transfer*, vol. 40, no. 18, pp. 4329−4335, 1997.

[9] J.-Y. Jang, J.-R. Ni, "Transient free convection with mass transfer from an isothermal vertical flat plate embedded in a porous medium," *International Journal of Heat and Fluid Flow*, vol. 10, no. 1, pp. 59−65, 1989.

[10] A. Bejan, K. R. Khair, "Heat and mass transfer by natural convection in a porous medium," *International Journal of Heat and Mass Transfer*, vol. 28, no. 5, pp. 909−918, 1985.

[11] D. Angirasa, G. P. Peterson, I. Pop, "Combined heat and mass transfer by natural convection with opposing buoyancy effects in a fluid saturated porous medium," *International Journal of Heat and Mass Transfer*, vol. 40, no. 12, pp. 2755−2773, 1997.

[12] I. Pop, H. Herwig, "Transfer mass transfer from an isothermal vertical flat plate embedded in a porous medium," *International Communications in Heat and Mass Transfer*, vol. 17, no. 6, pp. 813−821, 1990.

[13] C. Allain, M. Cloitre, A. Mongruel, "Scaling in flows driven by heat and mass convection in a porous medium," *Europhysics Letters*, vol. 20, no. 4, pp. 313−318, 1992.

[14] M. A. El-Hakiem, M. F. El-Amin, "Mass transfer effects on the non-Newtonian fluids past a vertical plate embedded in a porous medium with non-uniform surface heat flux," *Heat and Mass Transfer*, vol. 37, no. 2−3, pp. 293−297, 2001.

[15] R. Tsai, J. S. Huang, "Numerical study of Soret and Dufour effects on heat and mass transfer from natural convection flow over a vertical porous medium with variable wall heat fluxes," *Computational Materials Science*, vol. 47, no. 1, pp. 23−30, 2009.

[16] C.-Y. Cheng, "Natural convection heat and mass transfer of non-Newtonian power law fluids with yield stress in porous media from a vertical plate with variable wall heat and mass fluxes," *International Communications in Heat and Mass Transfer,* vol. 33, no. 9, pp. 1156−1164, 2006.

[17] M. K. Partha, P. V. S. N. Murthy, G. P. Raja Sekhar, "Soret and Dufour effects in a non-Darcy porous medium," *ASME Journal of Heat Transfer*, vol. 128, no. 6, pp. 605−610, 2006.

[18] R. R. Kairi, P. A. L. Narayana, P. V. S. N. Murthy, "The effect of double dispersion on natural convection heat and mass transfer in a non-Newtonian fluid saturated non-Darcy porous medium," *Transport in Porous Media*, vol. 76, no. 3, pp. 377−390, 2009.

[19] P. Singh, K. Tewari, "Non-Darcy free convection from vertical surfaces in thermally stratified porous media," *International Journal of Engineering Science*, vol. 31, no. 9, pp. 1233−1242, 1993.

[20] I. Y. Hussain, B. K. Raheem, "Natural convection heat transfer from a plane wall to thermally stratified porous media," *International Journal of Computer Applications*, vol. 65, no. 1, pp. 42−49, 2013.

[21] P. Singh, K. Sharma, "Integral method to free convection in thermally stratified porous medium," *Acta Mechanica*, vol. 83, no. 3−4, pp. 157−163, 1990.

[22] P. A. Lakshmi Narayana, P. V. S. N. Murthy, "Free convective heat and mass transfer in a doubly stratified non-Darcy porous medium," *ASME Journal of Heat Transfer* , vol. 128, no. 11, pp. 1204−1212, 2006.

[23] S. W. Armfield, J. C. Patterson, W. Lin, "Scaling investigation of the natural convection boundary layer on an evenly heated plate," *International Journal of Heat and Mass Transfer*, vol. 50, no. 7-8, pp. 1592-1602, 2007.

[24] A. Bejan, *Convection Heat Transfer*. New York: Wiley, 1995, pp. 18−21, pp. 535-539.

[25] C. A. J. Fletcher, *Computational Techniques for Fluid Dynamics 1. Fundamental and General Techniques.* New York: Springer-Verlag, 1991, pp. 296-299.

[26] J. C. Tannehill, D. A. Anderson, R. H. Pletcher, *Computational Fluid Mechanics and Heat Transfer*. Washington: Taylor&Francis, 1997, ch 3.

[27] O. V. Trevisan, A. Bejan, "Natural convection with combined heat and mass transfer buoyancy effects in a porous medium," *International Journal of Heat and Mass Transfer*, vol. 28, no. 8, pp. 1597-1611, 1985.

[28] D. Getachew, D. Poulikakos, W. J. Minkowycz, "Double diffusion in a porous cavity saturated with non-Newtonian fluid," *Journal of Thermophysics and Heat Transfer*, vol. 12, no. 3, pp. 437−446, 1998.

[29] R. Bennacer, A. Tobbal, H. Beji, P. Vasseur, "Double diffusive convection in a vertical enclosure filled with anisotropic porous media," *International Journal of Thermal Sciences*, vol. 40, no. 1, pp. 30-41, 2001.